Characterization and separation of *Cryptosporidium* and *Giardia* cells using on-chip dielectrophoresis

Harikrishnan Narayanan Unni,[1,a),b)] Deny Hartono,[2,b)] Lin Yue Lanry Yung,[2] Mary Mah-Lee Ng,[3] Heow Pueh Lee,[1] Boo Cheong Khoo,[1] and Kian-Meng Lim[1]

[1]*Department of Mechanical Engineering, National University of Singapore, 21, Lower Kent Ridge Road, Singapore 119077, Singapore*
[2]*Department of Chemical and Biomolecular Engineering, National University of Singapore, 21, Lower Kent Ridge Road, Singapore 119077, Singapore*
[3]*Department of Microbiology, National University of Singapore, 21, Lower Kent Ridge Road, Singapore 119077, Singapore*

(Received 26 August 2011; accepted 29 November 2011; published online 15 March 2012)

Dielectrophoresis (DEP) has been shown to have significant potential for the characterization of cells and could become an efficient tool for rapid identification and assessment of microorganisms. The present work is focused on the trapping, characterization, and separation of two species of *Cryptosporidium* (*C. parvum* and *C. muris*) and *Giardia lambia* (*G. lambia*) using a microfluidic experimental setup. *Cryptosporidium* oocysts, which are 2-4 μm in size and nearly spherical in shape, are used for the preliminary stage of prototype development and testing. *G. lambia* cysts are 8–12 μm in size. In order to facilitate effective trapping, simulations were performed to study the effects of buffer conductivity and applied voltage on the flow and cell transport inside the DEP chip. Microscopic experiments were performed using the fabricated device and the real part of Clausius—Mossotti factor of the cells was estimated from critical voltages for particle trapping at the electrodes under steady fluid flow. The dielectric properties of the cell compartments (cytoplasm and membrane) were calculated based on a single shell model of the cells. The separation of *C. muris* and *G. lambia* is achieved successfully at a frequency of 10 MHz and a voltage of 3 Vpp (peak to peak voltage). © *2012 American Institute of Physics*. [doi:10.1063/1.3671065]

I. INTRODUCTION

Dielectrophoresis (DEP) is an established technique for sorting, trapping, and characterizing cells and biomolecules.[1–3] DEP force acts on polarizable particles suspended in fluids and provides us with several key parameters, such as voltage, phase, and frequency of the AC current used, to control the manipulation process. It is possible to trap, characterize, and separate particles with different polarizabilities by tuning the abovementioned parameters. More recently, considerable attention has been paid to the potential of DEP as an analytical technique capable of providing information about the electrical parameters of cell compartments.[2,4–7] These parameters, especially permittivity and conductivity of cytoplasm and membrane, are linked to important physiological characteristics of the cell and can be deduced from real part of the characteristic Clausius-Mossotti factor, $\mathrm{Re}(f_{\mathrm{CM}})$. For that, two requisites have to be met: (1) the experimental measurements of cell motion or cell trapping voltage have to be related to $\mathrm{Re}(f_{\mathrm{CM}})$ values, and (2) an appropriate dielectric model of the cell that expresses $\mathrm{Re}(f_{\mathrm{CM}})$ in terms of electrical and geometric parameters of the cell has to be established.

[a)]Author to whom correspondence should be addressed. Electronic mail: mpehnu@nus.edu.sg.
[b)]Harikrishnan Narayanan Unni and Deny Hartono contributed equally to this work.

Dielectrophoresis has been shown to have significant potential for the characterization of cells and could become an efficient tool for rapid identification and assessment of microorganisms. Milner *et al.*[8] proposed a technique based on impedance measurement combined with DEP for analysis of bacteria. Suehiro *et al.*[9] subsequently applied a similar technique for selective detection of viable *Escherichia coli* bacteria, collecting them by means of interdigitated electrodes and assuming the measured conductance between electrodes to be proportional to the number of collected cells. Meanwhile, a DEP technique was used by Johari *et al.*[7] for obtaining and interpreting collection spectra of antibiotic-sensitive and antibiotic-resistant strains of *Staphylococcus epidermidis*. A simple experimental setup using sharp needle electrodes immersed in a static suspension was employed to interpret the number of collected cells as proportional to dielectric polarizability values. Later, Sanchis *et al.*[10] improved on the above two methods by (1) assuming a rod shape model for *E. coli* bacteria and (2) using a microelectrode chamber containing interdigitated electrodes through which the cell suspension circulates and a direct cell counting method by an image analysis system. Dielectric parameters of the cell compartments of *E. coli* and *Staphylococcus aureus* bacteria were determined using the above approach.

Cryptosporidium parvum is a protozoan parasite which produces oocysts as the infective stage in its life cycle. Ingestion of very low numbers of oocysts is considered sufficient to cause diarrheal illness in humans[11] which can be fatal in the immunosuppressed.[12] *Giardia lambia* is also a protozoan parasite which colonizes in the small intestine, producing *Giardiasis* (diarrheal infection of the small intestine). The *Cryptosporidium* oocysts are nearly spherical in shape[13] while the *Giardia* cells are spheroidal. The present work is focused on the trapping and characterization of *Cryptosporidium* and *Giardia* cells using a microfluidic experimental setup. In this study, the experimental setup is based on the integration of microfluidics within a microfabricated electrode set, with potentially easy integration into lab-on-a-chip systems for clinical or research purposes. A two compartment model of the pathogen cells (consisting of inner cytoplasm and plasma membrane) is presented in order to relate the real part of Clausius—Mossotti (CM) factor $\mathrm{Re}(f_{\mathrm{CM}})$ to the dielectric and geometric parameters of the cell compartments. The separation of *Cryptosporidium muris* and *Giardia lambia* cells is achieved successfully corresponding to a frequency of 10 MHz, at which the two cells show opposing dielectric behavior.

II. THEORY

Figure 1 shows the schematic of the single shell model of the *Cryptosporidium* and *Giardia* cells. *Cryptosporidium* cells are represented by a single shelled sphere while the *Giardia* cells are represented by a spheroidal shell. The inner layer represents the cytoplasm while the outer layer represents the plasma membrane. The component permittivity and conductivity of cytoplasm and membrane are represented by $(\varepsilon_1, \sigma_1)$ and $(\varepsilon_2, \sigma_2)$, respectively. The dielectric parameters of the external medium are represented by $(\varepsilon_3, \sigma_3)$. The dielectrophoretic force on such a composite cell is given as[14]

$$F_{DEP} = 2\pi\varepsilon_m a_p^3 \mathrm{Re}(f_{\mathrm{CM}})\nabla|\boldsymbol{E}|^2, \tag{1}$$

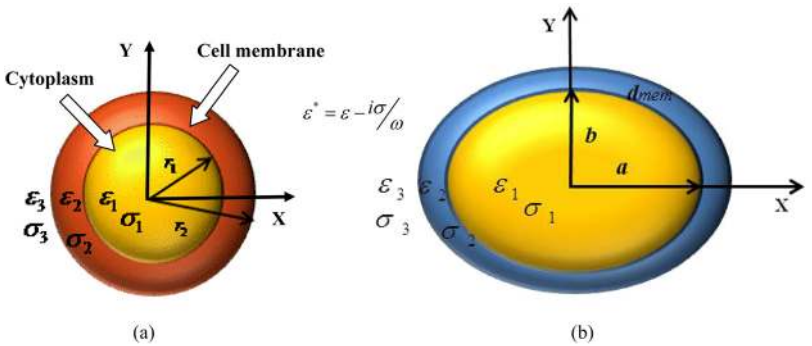

FIG. 1. Schematic model of the *Cryptosporidium* (sphere) and *Giardia* (spheroid) cells.

where ε_m represents the dielectric permittivitty of the medium, a_p represents the cell radius, and $\boldsymbol{E}$ is the applied electric field. The characteristic CM factor for the case of spherical shells cell can be expressed as

$$f_{\mathrm{CM}} = \frac{\varepsilon^*_{eff} - \varepsilon^*_3}{\varepsilon^*_{eff} + 2\varepsilon^*_3}, \text{where } \varepsilon^*_{eff} = \varepsilon^*_2 \left[\frac{\left(\frac{r_2}{r_1}\right)^3 + 2\frac{\varepsilon^*_1 - \varepsilon^*_2}{\varepsilon^*_1 + 2\varepsilon^*_2}}{\left(\frac{r_2}{r_1}\right)^3 - \frac{\varepsilon^*_1 - \varepsilon^*_2}{\varepsilon^*_1 + 2\varepsilon^*_2}} \right]. \tag{2}$$

In the above equation, r_1 and r_2 represent the inner and outer radius of the spherical shell and the complex permittivity,

$$\varepsilon^*_k = \left(\varepsilon_k - i\frac{\sigma_k}{\omega}\right) \text{ and } k = 1, 2, 3. \tag{3}$$

In the above expression, $\omega = 2\pi f$, is the angular frequency of the applied electric field.

As Eq. (1) is only applicable for spherical cells, it is essential to modify the CM factor taking into account of the spheroidal shape of the cells.[15] This consideration defines the three components of this factor for the three possible axes of polarization that in the case of homogeneous ellipsoids are expressed as

$$P_i = \frac{1}{3}\frac{\left(\varepsilon^*_p - \varepsilon^*_m\right)}{\varepsilon^*_m + A_i\left(\varepsilon^*_p - \varepsilon^*_m\right)}, \tag{4}$$

where ε^*_p and ε^*_m represent the homogeneous cell permittivity and the medium permittivity, respectively. In Eq. (4), A_i is a component of the depolarization factor along any one of three axes of the ellipsoid ($i = x, y, z$). A_i is expressed as[16]

$$A_i = \frac{abc}{2}\int_0^\infty \frac{ds}{\left(s + q_i^2\right)\sqrt{(a^2 + s)(b^2 + s)(c^2 + s)}}, \tag{5}$$

where a, b, and c represent the three minor axes of the ellipsoid and $q_i = a, b, c$ for $i = x, y, z$.

In the special case of a prolate spheroid, $a > b = c$, and the depolarization component at the direction of its major axis (symmetric axis) is given by

$$A_x = \frac{(1 - e^2)}{2e^3}\left[\log\frac{1 + e}{1 - e} - 2e\right], \tag{6}$$

where $e = \sqrt{1 - \left(\frac{b}{a}\right)^2}$ is the eccentricity of the spheroid. In this expression, a and b refer to the semi-major and semi-minor axis lengths of the spheroidal cell (depicted in Figure 1(b)). However, the biological cell is not homogeneous and is represented as a shell having a cytoplasm and membrane with different dielectric properties (as depicted in Figure 1(b)). The DEP behavior of the transport of such a spheroidal cell along X-axis can be expressed using the directional CM factor,

$$f_{CM_x} = \frac{1}{3}\frac{\left(\varepsilon^*_2 - \varepsilon^*_3\right) + 3P_x\rho_1\left[\varepsilon^*_2 + A_{2x}\left(\varepsilon^*_2 - \varepsilon^*_3\right)\right]}{\left[\varepsilon^*_3 + A_{2x}\left(\varepsilon^*_2 - \varepsilon^*_3\right)\right] + 3P_x\rho_1 A_{2x}(1 - A_{2x})\left(\varepsilon^*_2 - \varepsilon^*_3\right)}, \tag{7}$$

where the cell polarization factor, P_x is expressed as

$$P_x = \frac{1}{3}\frac{\left(\varepsilon^*_1 - \varepsilon^*_2\right)}{\varepsilon^*_2 + A_{1x}\left(\varepsilon^*_1 - \varepsilon^*_2\right)}. \tag{8}$$

In Eq. (7), f_{CM_x} represents the cell CM factor for X-axis of polarization (the direction of cell transport in the present study).

In the above equations, A_{1x} and A_{2x} represents the cell eccentricity factors,

$$A_{1x} = \frac{(1-e_1^2)}{2e_1^3}\left[\log\frac{1+e_1}{1-e_1} - 2e_1\right] \quad e_1 = \sqrt{1-\left(\frac{b}{a}\right)^2}$$

$$A_{2x} = \frac{(1-e_2^2)}{2e_2^3}\left[\log\frac{1+e_2}{1-e_2} - 2e_2\right] \quad e_2 = \sqrt{1-\left(\frac{b+d_{mem}}{a+d_{mem}}\right)^2}$$

In the above expressions, A_{1x} and A_{2x} represent the x-component of depolarization for the inner cytoplasm layer and the layer including the cytoplasm and cell membrane, respectively.

ρ_1 is expressed as

$$\rho_1 = \frac{ab^2}{(a+d_{mem})(b+d_{mem})^2}, \tag{9}$$

d_{mem} represents the thickness of the cell membrane. As $A_x + A_y + A_z = 1$ and due to rotational symmetry of the spheroidal cell, the CM factor in the Y and Z directions can be expressed according to Eqs. (7) and (8) by using expressions $A_{1,y} = A_{1,z} = (1 - A_{1,x})/2$, $A_{2,y} = A_{2,z} = (1 - A_{2,x})/2$.

The averaged CM factor of the cell is then expressed as

$$f_{\mathrm{CM}} = \frac{1}{3}\sum_{i=x,y,z}(f_{CMi}). \tag{10}$$

Using Eq. (3) in Eq. (2) and expanding, the real part of the effective CM factor of a spherical cell can be written as

$$\mathrm{Re}(f_{\mathrm{CM}}) = \frac{\left[\varepsilon_2\frac{(p+s)}{t} + \frac{\sigma_2}{\omega}\frac{(q-r)}{t} - \varepsilon_3\right]^2 + 3\varepsilon_3\left[\varepsilon_2\frac{(p+s)}{t} + \frac{\sigma_2}{\omega}\frac{(q-r)}{t} - \varepsilon_3\right]}{\left[\varepsilon_2\frac{(p+s)}{t} + \frac{\sigma_2}{\omega}\frac{(q-r)}{t} + 2\varepsilon_3\right]^2 + \left[\varepsilon_2\frac{(q-r)}{t} - \frac{\sigma_2}{\omega}\frac{(p+s)}{t} - \frac{2\sigma_3}{\omega}\right]^2}, \tag{11}$$

where the terms p, q, r, s, and t in Eq. (11) are expressed as

$$\begin{aligned}
p &= \gamma^6(\varepsilon_1+\varepsilon_2)(\varepsilon_1+2\varepsilon_2) - \gamma^3(\varepsilon_1-\varepsilon_2)(\varepsilon_1+2\varepsilon_2) + 2\gamma^3(\varepsilon_1^2-\varepsilon_2^2) - 2(\varepsilon_1-\varepsilon_2)^2,\\
q &= \gamma^6\frac{(\varepsilon_1+2\varepsilon_2)(\sigma_1+2\sigma_2)}{\omega} - \gamma^3\frac{(\varepsilon_1+2\varepsilon_2)(\sigma_1-\sigma_2)}{\omega} + 2\gamma^3\frac{(\varepsilon_1-\varepsilon_2)(\sigma_1+2\sigma_2)}{\omega} - \frac{2(\varepsilon_1-\varepsilon_2)(\sigma_1-\sigma_2)}{\omega},\\
r &= \gamma^6\frac{(\sigma_1+\sigma_2)(\varepsilon_1+2\varepsilon_2)}{\omega} - \gamma^3\frac{(\varepsilon_1-\varepsilon_2)(\sigma_1+2\sigma_2)}{\omega} + 2\gamma^3\frac{(\varepsilon_1+2\varepsilon_2)(\sigma_1-\sigma_2)}{\omega} - \frac{2(\varepsilon_1-\varepsilon_2)(\sigma_1-\sigma_2)}{\omega},\\
s &= \gamma^6\frac{(\sigma_1+2\sigma_2)^2}{\omega^2} - \gamma^3\frac{(\sigma_1+2\sigma_2)(\sigma_1-\sigma_2)}{\omega^2} + 2\gamma^3\frac{(\sigma_1-\sigma_2)(\sigma_1+2\sigma_2)}{\omega^2} - \frac{2(\sigma_1-\sigma_2)^2}{\omega^2},\\
t &= \gamma^6(\varepsilon_1+2\varepsilon_2)^2 + (\varepsilon_1-\varepsilon_2)^2 - 2\gamma^3(\varepsilon_1+2\varepsilon_2)(\varepsilon_1-\varepsilon_2) + \gamma^6\frac{(\sigma_1+2\sigma_2)^2}{\omega^2} + \frac{(\sigma_1-\sigma_2)^2}{\omega^2}\\
&\quad - 2\gamma^3\frac{(\sigma_1+2\sigma_2)(\sigma_1-\sigma_2)}{\omega^2}.
\end{aligned} \tag{12}$$

In the above expressions, $\gamma = \frac{r_2}{r_1}$.

Substituting p, q, r, s, and t into Eq. (11) will result in a high order polynomial expression of $\mathrm{Re}(f_{\mathrm{CM}})$ in terms of $(\varepsilon_1, \sigma_1)$, $(\varepsilon_2, \sigma_2)$, and $(\varepsilon_3, \sigma_3)$. Through a similar procedure, though tedious, the CM factor of a spheroidal cell can be expressed in terms of the cell and medium

dielectric parameters. After obtaining the distributions of the electrical field and flow field separately, the region where a cell can be trapped can be found.

The hydrodynamic force on a spherical cell near to a plane boundary is expressed as[17]

$$F_H = 6\pi\mu a U f_H, \tag{13}$$

where U is the fluid velocity and μ is the dynamic viscosity of the fluid medium. The factor f_H represents the hydrodynamic correction function to account for the near wall effects due to the presence of the plane boundary. Expression for f_H for the case of motion of a sphere near a plane boundary is given in Ref. 17. In order for the cell to be trapped, the maximum DEP force on the cell should be greater than or equal to the hydrodynamic drag on the cell.

The correction factor for a prolate spheroidal shell is expressed as

$$F_H = 6\pi\mu b U f_1 f_2, \tag{14}$$

where f_1 is the spheroid is shape factor and f_2 is the boundary correction factor,[17]

$$f_1 = \frac{\frac{4}{3}\left(\beta^2 - 1\right)}{\frac{\left(2\beta^2 - 1\right)}{\sqrt{\beta^2 - 1}} \ln\left[\beta + \sqrt{\beta^2 - 1}\right] - \beta}, \quad \beta = a/b, \tag{15}$$

$$f_2 = \frac{b(K + a^2/L_1)}{\pi\left[1 - 0.554\left(\frac{b}{l}\right) + 0.1092\left(\frac{b}{l}\right)^3 - 0.023\left(\frac{b}{l}\right)^4\right]}, \tag{16}$$

where l is the cell centre to channel wall separation distance and

$$K = \int_0^\infty \frac{ds}{\sqrt{(a^2 + s)(b^2 + s)(c^2 + s)}}, \quad L_1 = \int_0^\infty \frac{ds}{(a^2 + s)\sqrt{(a^2 + s)(b^2 + s)(c^2 + s)}}. \tag{17}$$

In the case of a spheroid, $b = c$.

Equating the DEP and hydrodynamic forces on a spherical cell results in an expression for the real part of CM factor

$$\mathrm{Re}(f_{\mathrm{CM}}) = \frac{3\mu U f_H}{\varepsilon_m a^2 \nabla |E|_x^2}. \tag{18}$$

Similarly, the real part of CM factor for a spheroidal cell can be expressed as

$$[\mathrm{Re}(f_{\mathrm{CM}})]_x = \mathrm{Re}(f_{CM_x}) = \frac{3\mu U f_1 f_2}{\varepsilon_m b^2 \nabla |E|_x^2}, \tag{19}$$

where $|E|_x$ represents the component of the applied field in the x direction. In the case of spheroidal cell, the x direction is along the major axis of the cell. Therefore, the real part of CM factor can be calculated once the electric field distribution is calculated corresponding to the experimentally determined critical voltages of cell trapping and release at different frequencies.

The flow field velocity, U is determined by the governing Navier-Stokes equation. In the present case of flow over an electrode array, the flow field will depend on the electrothermal force arising from Joule heating at the electrodes. The corresponding governing equations for the electrical, thermal, and flow fields are given as follows:

$$\nabla^2 \Phi = 0, \boldsymbol{E} = -\nabla\Phi, \nabla \cdot (-k\nabla T) = \sigma |\boldsymbol{E}|^2 - \rho C_p U \cdot \nabla T, \tag{20}$$

$$\nabla p - \mu \nabla^2 U + \rho U \cdot \nabla U = \boldsymbol{f}_{ET}, \tag{21}$$

where Φ represents the electrical potential and T is the temperature. The electrothermal force can be expressed as[18]

$$\boldsymbol{f}_{ET} = -0.5\left[\left(\frac{\nabla\sigma}{\sigma} + \frac{\nabla\varepsilon}{\varepsilon}\right) \cdot \boldsymbol{E}\frac{\varepsilon \boldsymbol{E}}{1 + (\omega\tau)^2} + 0.5|\boldsymbol{E}|^2 \nabla\varepsilon\right], \tag{22}$$

where $\tau = \frac{\varepsilon}{\sigma}$ is the fluid's charge-relaxation time. The coupled field equations represented by Eqs. (20) and (21) are solved using COMSOL MULTIPHYSICS.

III. MATERIALS AND FABRICATION

The interdigitated electrodes (of width 30 μm) of the microfluidic device are fabricated from indium tin oxide (ITO) coated glass slides. These glass slides provide high transparency and good electrical conductivity, enabling visualization of the flow of cells in the microchannel. The ITO glass slides were first cleaned by rinsing with isopropanol, acetone, and deionized water, blow-dried with compressed air, and then dehydrated on a hot plate at 100 °C for 10 min. A positive-tone photoresist AZ2001 is spun-coated at 2500 rpm for 20 s with an acceleration of 300 rpm/s, and the slide was baked at 95 °C for 90 s prior to standard photolithography. The slide was then exposed to ultraviolet light at about 80 mJ/cm2 (Karl Suss MA4 Mask Aligner, Waterbury, VT) through a film mask (IGI, Singapore). Subsequently, the slide was immersed into a solution of AZ400K developer and deionized water (1:4) for 20 s. The slide is then etched in a solution of ferric chloride (35 g), hydrochloric acid (250 ml), and deionized water (250 ml). The etching time in our experiment is about 10 min. After the etching process, the slide was rinsed with acetone and water to remove the photoresist and finally blow-dried.

PDMS replicas of microchannels were fabricated by standard lithographic patterning of channel designs on Si wafer using SU8 50 photoresist. The width and depth of the channels were 1 mm and 25 μm, respectively. In order to enhance the bonding between PDMS and ITO, the ITO glass plate was coated with an alkoxysilane solution DMOAP (N, N—dimethyl-N-octadecyl-3-aminopropyltrimethoxysilyl chloride) prior to bonding. The silane coating was found to enhance the bonding between ITO and PDMS and reduces cell adhesion on the electrodes. In order to coat the silane solution, the ITO substrate was cleaned with acetone and DI water followed by dipping the substrate in 1% solution of DMOAP in water. The substrate was agitated at room temperature for 5 min and subsequently rinsed with DI water and blow dried with N_2. The ITO substrate was later cured at 110 °C for 1 h. The PDMS channel and coated ITO glass plate were plasma bonded (2 min) to form the microfluidic chip.

IV. EXPERIMENT

The schematic of the experimental setup is presented in Figure 2. Suspensions of *Cryptosporidium* and *Giardia* cells with a concentration of 3×10^6/ml were prepared and pumped into the microfluidic device using a syringe pump. The flow rate in the present experiment was maintained at a steady rate of 0.01 ml/h, which corresponds to a flow velocity of nearly 1.7×10^{-4} m/s in the microchannel. Conductive epoxy was deposited on the electrode leads in the ITO glass plate and the leads were subsequently connected to a function generator using platinum wires. AC voltages of different amplitudes and frequency were applied to the electrodes in order to determine the optimum voltage for trapping and release of cells. Figure 3 shows the cells trapped at the edges of the electrodes. The cells are trapped by the strip electrodes when a sufficiently high voltage is applied and the maximum DEP force is greater than the hydrodynamic force from the flowing fluid. In our experiments, the cells are first trapped at the strip electrodes (with a voltage of 10 Vpp). The voltage is then lowered slowly until a critical value where the cells are just released and start to flow away. At this critical voltage, the

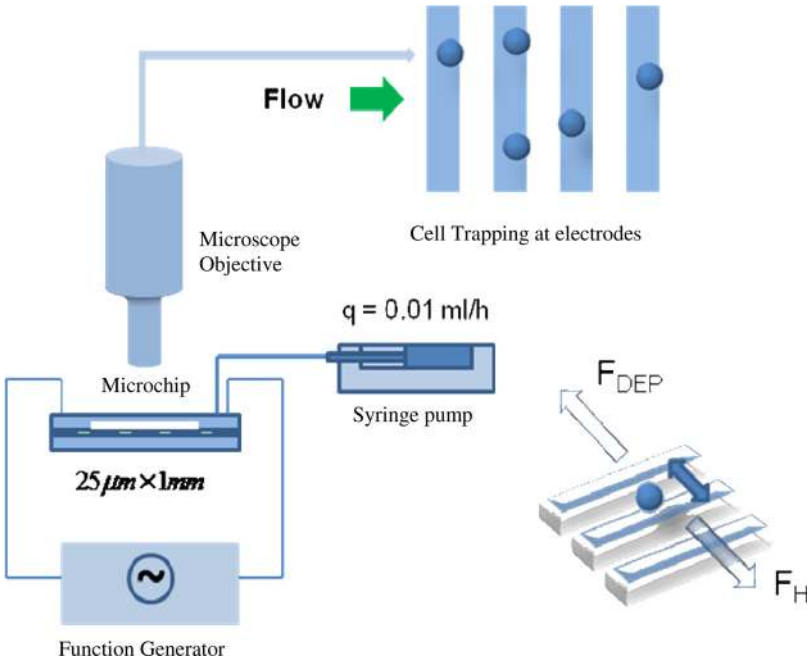

FIG. 2. Schematic of the video microscopic experimental setup for cell trapping.

maximum DEP force is just equal to the hydrodynamic force. The critical voltage corresponding to cell release was noted for various frequencies ranging from 10 kHz to 20 MHz. The electric field distribution corresponding to this critical voltage was obtained by numerical simulation of Laplace equation represented in Eq. (20) and the real part of CM factor was calculated according to Eqs. (18) and (19).

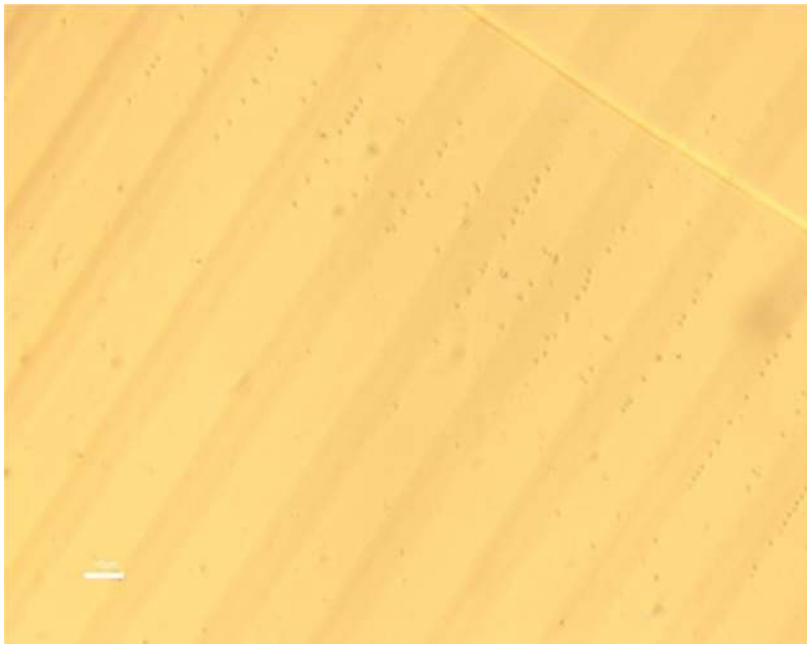

FIG. 3. Trapped *Cryptosporidium* cells at the electrodes. The applied voltage is 5 Vpp and frequency is 200 kHz.

V. RESULTS AND DISCUSSION

A. Microfluidic design and operating parameters

Figures 4(a) and 4(b) represent the electrothermal flow fields in the microchannel simulated using Eqs. (20) and (21). For the case of $\sigma = 0.1$ S/m and V = 10 Vpp (peak to peak voltage), localized recirculation flows are noticed, with an enhancement of flow velocity in the vicinity of the electrodes. This flow behavior can be attributed to the higher conductivity of the buffer solution, as the magnitude of localized Joule heating is proportional to the buffer conductivity. The resulting electrothermal force governs the electro-hydrodynamic flow in the vicinity of the electrodes. These localized flow vortices are undesirable in the experiment, as they could affect the trapping at the electrodes, resulting in unstable trapping. In the case of lower conductivity buffer solutions ($\sigma = 10^{-4}$ S/m), the magnitude of electrothermal force is negligible, and the flow in the vicinity of the electrode is not affected. Therefore, deionized water ($\sigma = 5.5 \times 10^{-6}$ S/m) was chosen as the buffer solution for the experiments. The applied field is important as well, as the magnitude of

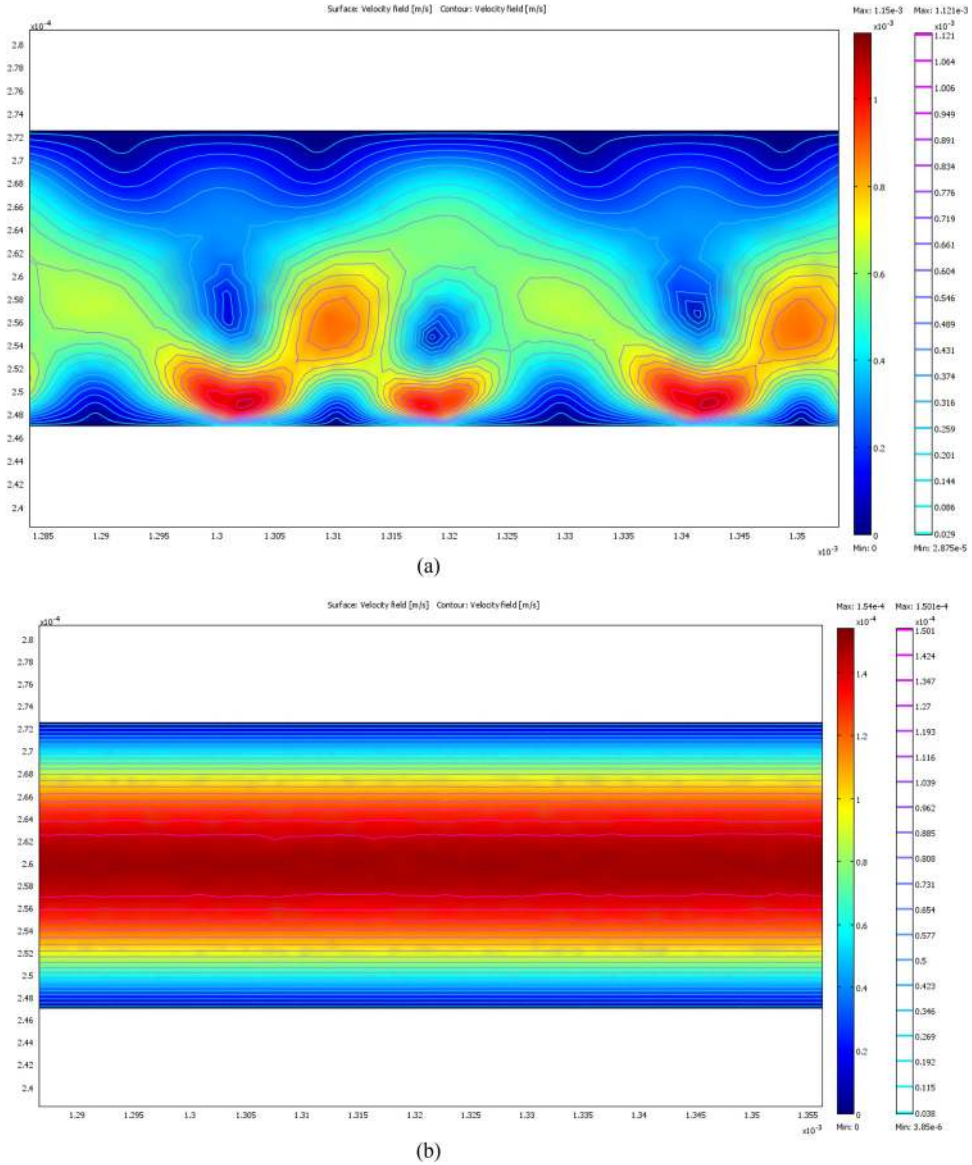

FIG. 4 (a). Electrothermal flow field corresponding to an applied voltage of 10 Vpp and $\sigma = 0.1$ S/m. (b) Electrothermal flow field corresponding to an applied voltage of 10 Vpp and $\sigma = 10^{-3}$ S/m.

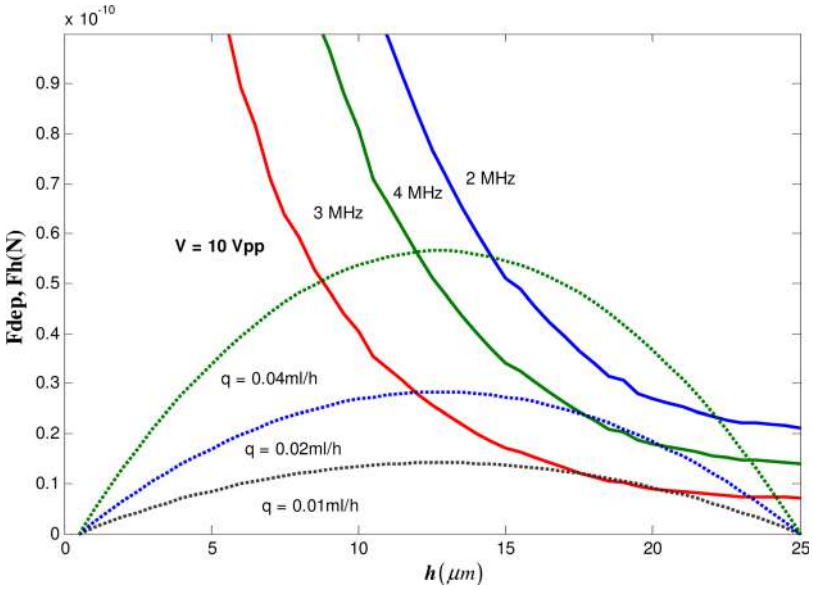

FIG. 5. DEP and hydrodynamic forces on a *Cryptosporidium* oocyst cell in a microfluidic channel of height h = 25 μm.

localized Joule heating is proportional to $|\boldsymbol{E}|^2$. In our experiments, the maximum value of applied voltage was below 10 Vpp ($V_{rms} < 3.3$ V) so that the electrothermal forces calculated using Eq. (22) were negligible and it is safe to assume that there are no local flow disturbances and thermal effects on the cells. As DEP force decays quickly within a few micrometers distance from the electrodes, the channel height becomes a significant parameter in the microfluidic trap design. The channel height of the device used in the present experiments was chosen to be 25 μm. The variation of DEP and hydrodynamic forces across a channel of height 25 μm is presented in Figure 5. For the simulations of DEP and hydrodynamic forces, the cell diameter was assumed to be 2 μm as the *Cryptosporidium* oocyst cells are observed to be around 2 μm in diameter during experiments, and $\mathrm{Re}(f_{\mathrm{CM}})$ was initially calculated from the extracted values of cell dielectric parameters (presented in Table I) based on electrotation spectra of *Cryptosporidium* presented in the work of Goater *et al.*[19] On the other hand, *Giardia* cells are observed to be larger, having a major axis diameter of 10μm and minor axis diameter of 4 μm, so that the magnitude of DEP forces would be stronger on these cells. It can be observed that the DEP force is strong enough to trap the cells along the entire height of the channel, when the flow rate q = 0.01 ml/h (which is used in our experiments) and V = 10 Vpp, at sample field frequencies of 2 MHz, 3 MHz, and 4 MHz.

B. Frequency spectrum of the critical voltage

The critical voltage corresponding to the release of the two different type of cells is plotted against the electric field frequency in Figures 6 and 7. The two *Cryptosporidium* cell species show only a qualitative difference in the dielectric behaviour for the range of frequencies studied. For *C. parvum*, two peak values of critical voltages of 7.8 V (averaged) and 4.7 V occur at about 3 MHz and 30 kHz. In the case of *C. muris* cells, peak critical voltage of 6.8 V and 4.8 V is achieved at about 3.1 MHz and about 30 kHz. Around these values of critical frequency, both the cells show opposing dielectric behaviour as observed from the increasing and decreasing trends of critical voltage observed in a frequency range of 30 kHz $< f <$ 5 MHz. A decreasing trend of critical voltage would mean an increase in the magnitude of DEP force and vice versa. Therefore, the trend of critical voltage can be understood by the fact that cells undergo both positive and negative DEP across a short frequency range around 30 kHz and 3 MHz. These frequencies can be referred to as the first and second critical frequencies (f_{c1} and f_{c2}) at which the real part of CM factor becomes equal to 0. This behaviour can be attributed to the dielectric permittivity and conductivity of the biological cells, being much higher than that of insulating

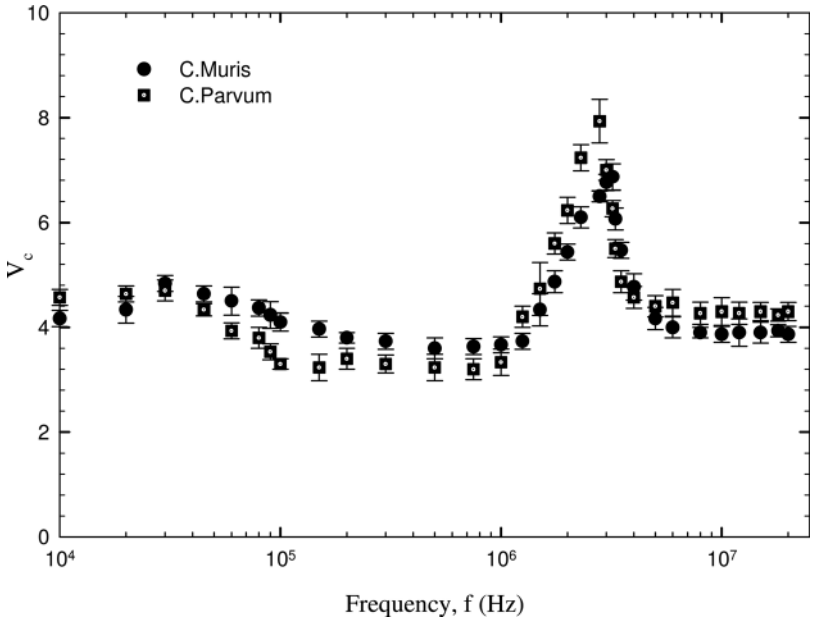

FIG. 6. Frequency spectrum of the critical Voltage of *Cryptosporidium* cell release.

particles such as latex (which always exhibit negative DEP in water). For *Cryptosporidium*, the DEP force nearly remains constant in the range of 100 kHz to 1 MHz as indicated by the near constant values of critical voltage in this range. A consistent negative DEP force is experienced by *Giardia* cells in the frequency range of 10 kHz to 1 MHz as indicated by the higher voltages of cell release. This indicates that, at lower frequencies, the cells are experiencing negative DEP, which alters to positive DEP at a critical frequency value of 1.5 MHz (first critical frequency, f_{c1}) and the values of f_{c2} is beyond 20 MHz. The frequency corresponding to the peak value of critical voltage indicates very low value of DEP force (positive or negative). For *Cryptosporidium* cells, the regime > 3 MHz indicates stronger negative DEP force, with the critical voltage required for particle release lowering to about 2 V. The *G. lambia* cells show opposite

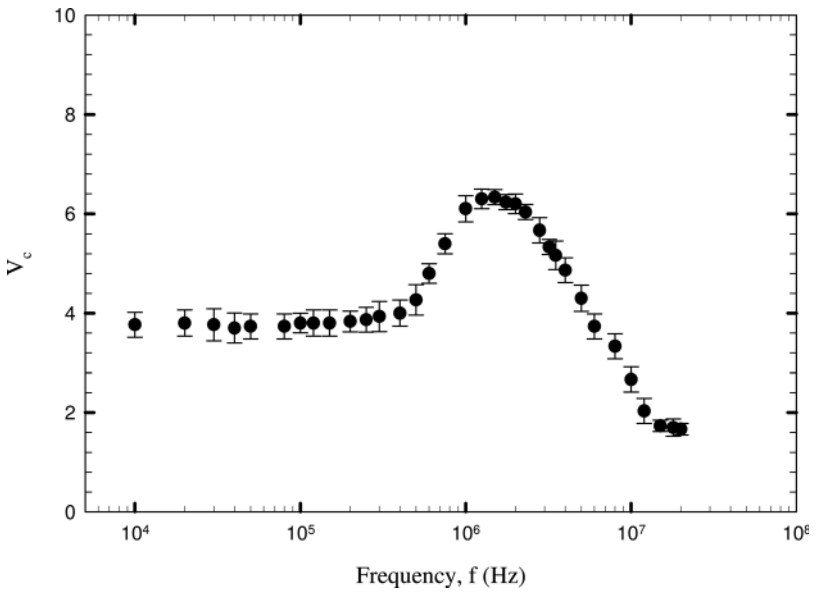

FIG. 7. Frequency spectrum of the critical Voltage of *Giardia* cell release.

dielectric behaviour from the *Cryptosporidium* cells as is observed from the higher values of critical voltages at low frequencies and lower values of critical voltages at higher frequencies. In effect, this means that in the proximity of a frequency value of 3 MHz, where both *Cryptosporidium* and *Giardia* cells show weak DEP forces, separation of cells would be difficult unless high values of voltages (in order to amplify the dielectric difference) are used.

C. Real part of CM factor and cell dielectric parameters

The real part of CM factor was calculated using Eqs. (18) and (19). The field gradient term $\nabla|E|_x^2$ was obtained by numerical simulation corresponding to the critical voltage values plotted in Figures 6 and 7. The hydrodynamic correction factor f_H, f_1, and f_2 were computed assuming that; (1) in the case of negative DEP, the cells are trapped and positioned one cell radius away from the top channel wall and (2) the case of positive DEP, the cells are trapped at the bottom electrodes. Figure 8 depicts the real part of CM factor of the three different cells corresponding to different field frequencies. The average values of V_c corresponding to each frequency was employed for calculation of Re(f_{CM}). From Figure 8, the cross over frequency (the frequency corresponding to Re(f_{CM}) = 0, which represents transition from positive to negative DEP) was estimated to be 3 MHz for *C. parvum* and 3.1 MHz for *C. muris*. This information is vital in the operation of pDEP traps and field flow fractionation (FFF) devices using nDEP levitation, as the regime of strong pDEP and nDEP forces can be determined from the CM factor plot. In the present case, *Cryptosporidium* cells experience a maximum pDEP force in a frequency range 100 kHz $< f <$ 1 MHz and a maximum nDEP force when $f >$ 4 MHz. The contrary becomes true in the case of *G. lambia* cells, with a stronger pDEP regime when $f >$ 3 MHz and a stronger nDEP regime when $f <$ 1 MHz.

Referring to Eqs. (11) and (12), $(\varepsilon_1, \sigma_1)$ and $(\varepsilon_2, \sigma_2)$ are the unknowns to be calculated as the medium permittivity $(\varepsilon_3, \sigma_3)$ is a known quantity. The thickness of the *Cryptosporidium* cell membrane layer can be assumed to be nearly 50 nm,[20] while the membrane thickness of *Giardia* cells are larger and assumed to be 400 nm.[21] Therefore, the radius ratio of the cells can be calculated. In order to generate equations for solving the unknowns, Re(f_{CM}) corresponding to the frequency values plotted in Figure 8 is expanded in terms of the cytoplasm and membrane dielectric parameters using Eqs. (11) and (12). After some algebraic manipulation, a set of highly nonlinear equations are obtained. These equations are solved by nonlinear least squares method to obtain a best fit. In addition, using the same technique, dielectric parameters of *C.*

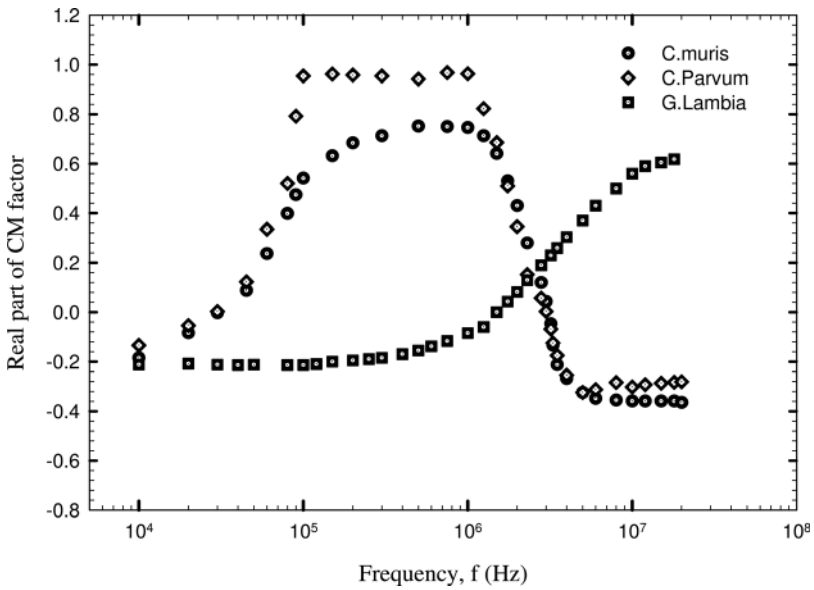

FIG. 8. Clausius-Mossotti factor of *Cryptosporidium* and *Giardia* cells.

TABLE I. *Cryptosporidium* dielectric properties compared to properties of other bacterial species.

	ε_{cyto}	ε_{mem}	σ_{cyto}	σ_{mem}
Present work—*C. parvum*	61.35	9.84	0.047	1.86×10^{-7}
Estimation based on results from the work of Goater *et al.*[19]—*C. parvum*	56.65	8.73	0.052	3.46×10^{-7}
Present work—*G. lambia*	65.58	12.11	0.016	2.47×10^{-6}
Present work—*C. muris*	60.46	4.39	0.052	0.95×10^{-7}
Sanchis *et al.*[10]—*E. Coli*	70 ± 10	10 ± 0.5	0.07 ± 0.01	$<1.5 \times 10^{-6}$
Sanchis *et al.*[10]—*S. aureus*	70 ± 10	16 ± 0.5	0.8 ± 0.05	$<1.5 \times 10^{-6}$
Suehiro *et al.*[9]—*E. coli*	60	10	0.1	5×10^{-8}

parvum were extracted from results of electrotation spectra presented in the work of Goater *et al.*,[19] after expressing for the cell electrorotational velocity in terms of the imaginary part of CM factor, $\mathrm{Im}(f_{\mathrm{CM}})$. The results from the present work and results based on Goater's work agree reasonably well. Table I shows the dielectric parameters of the cell compartments obtained in the present study compared with the results obtained for other Gram positive (*S. aureus*) and Gram negative (*E. coli*) bacteria from Sanchis *et al.*[10] and Johari *et al.*[7] Gram positive bacteria such as *S. aureus* has a significantly higher cytoplasm conductivity compared to the *Cryptosporidium*, which could be explained in line with the known fact that Gram positive bacteria have a higher K^+ content in their cytoplasm. As the two species have nearly the same size (1-2 μm cell radius), the difference in dielectric properties of the above two species may be utilized as a key parameter for separation of the two species *on-chip*. Conversely, the difference in dielectric permittivity and conductivity of *E. coli* (nearly 2 μm long rod shaped bacteria) and *Cryptosporidium* are relatively small, therefore, on-chip separation may not be feasible without the use of high electric fields, which in turn may damage the cells. However, the contrasting behaviour of the *G. lambia* and *C. muris*/*C. parvum* cells provide an interesting prospective of separating them *on-chip* at frequencies >5 MHz and frequencies <1 MHz. The dielectric parameters (especially, the conductivity value) obtained for the membrane layer are significantly lower compared to that of the cytoplasm layer. This can be attributed to the permeable and lipidic nature of the cell membrane and presence of metal ions in the cytoplasm. It has to be mentioned here that the present work is focused on a single shell model including a cell cytoplasm and plasma membrane. Further refinement in cell modelling will involve a double shell model, incorporating a three compartment structure: cytoplasm, plasma membrane, and cell wall. However, this will introduce additional mathematical complexity in the modelling and solving for the dielectric parameters.

D. On-chip separation of *C. muris* and *G. lambia*

Figure 9 shows the snapshots of the separation of *C. muris* and *G. lambia* cells (circled cells) at a frequency of 10 MHz and a voltage of 3 Vpp. The *Giardia* cells experience positive DEP at this frequency value and are strongly trapped at the electrodes. This is depicted by the blurred *C. muris* cells that are present in a different plane compared to *G. lambia* cells as they are levitated by nDEP. At this frequency, the *Cryptosporidium* cells require voltages in excess of 4 Vpp to be stably trapped by nDEP. In Figure 9, frame 1 shows both *C. muris* and *G. lambia* trapped on the electrode at $\mathrm{f} = 10$ MHz and 5 Vpp. Subsequently, the voltage is lowered to 3 Vpp and the remaining two snapshots at $t = 0.5$ s and $t = 1$ s shows the *C. muris* cells getting released from the electrode and moving while *G. lambia* cells remains on the electrode. At this voltage, the hydrodynamic forces on the *C. muris* cells overcome the nDEP force on the cells and results in the release of cells from the electrode. The pDEP force on the *Giardia* cells is strong enough to hold the cells on the electrode upto a voltage of 2 Vpp (as depicted in the critical voltage plot in Figure 7). On the other hand, for most of the frequency range, separation of *C. parvum* and *C. muris* cells will be a challenging task, as both these cells show only a

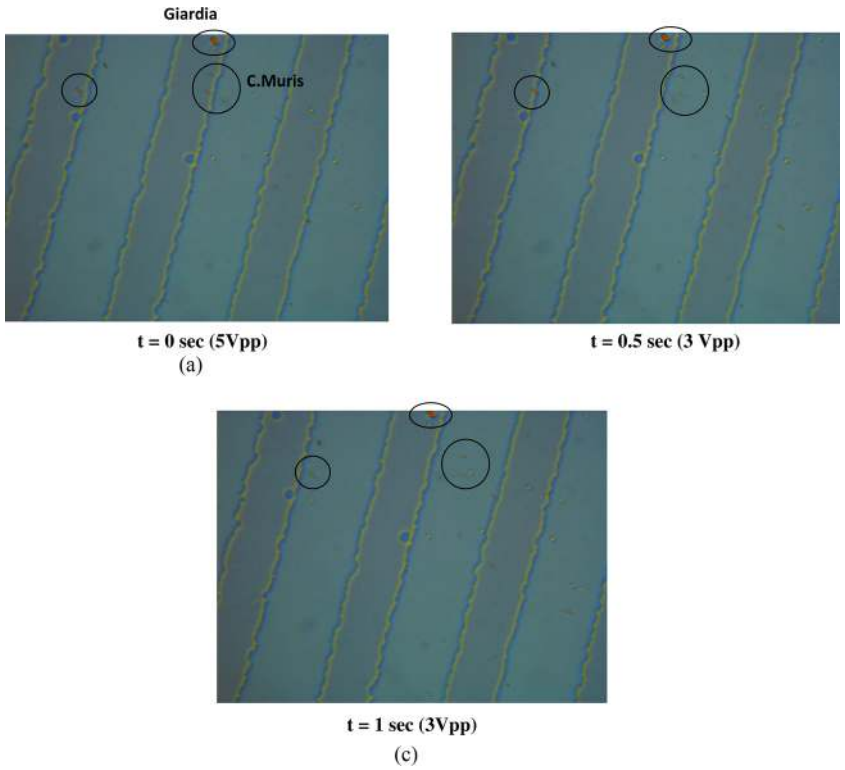

FIG. 9. Snapshots of separation of *G. lambia* and *C. muris* at 10 MHz.

minor quantitative difference in their dielectric properties, except for the region $200\,\text{kHz} < f < 1\,\text{MHz}$.

VI. CONCLUSIONS

The present work shows an efficient scheme for o*n-chip* trapping, characterization, and separation of pathogens on chip using DEP. The dielectric properties of the cytoplasm and membrane compartments of the cells were determined via the measurement of critical voltage corresponding to release of trapped cells from electrodes. The real part of CM factor was estimated from the critical voltage plot, in an effort to locate the DEP crossover frequency for the cells. Finally, the dielectric parameters of the cell compartments were estimated from the real part of CM factor. Separation of *C. muris* and *G. lambia* samples was achieved at a frequency of 10 MHz and voltage of 3 Vpp. In addition, the microdevice allows a rapid assessment of bacterial or other cell samples, with easy integration into lab-on-a chip systems for clinical or research purposes. The strong bonding between silane-coated ITO electrodes and PDMS allows repeated usage of the device for several hours of experimental duration.

ACKNOWLEDGMENTS

The authors greatly acknowledge the funding support from NRF (EWI), Singapore—Grant No. 0803-IRIS-02.

[1]H. Morgan and N. G. Green, J. Electrost. **42**, 279 (1997).
[2]M. P. Hughes, H. Morgan, F. J. Rixon, Biochim. Biophys. Acta **1571**, 1 (2002).
[3]K. S. Soumya, R. D. Prashant, C. B. Shane, and R. M. Adrienne, Electrophoresis **29**, 5033 (2008).
[4]J. Gimsa, "Characterization of particles and biological cells by AC electrokinetics," in *Interfacial Electrokinetics and Electrophoresis*, edited by A. V. Delgado (Marcel Dekker Inc., New York, 2001), pp. 369–400.
[5]R. Hozel, J. Electrost. **56**, 435 (2002).
[6]K. Ratanachoo, P. R. C. Gascoyne, and M. Ruchirawat, Biochim. Biophys. Acta **1564**, 449 (2002).
[7]J. Johari, Y. Hubner, J. C. Hull, J. W. Dale, and M. P. Hughes, Phys. Med. Biol. **48**, 193 (2003).

[8]K. R. Milner, A. P. Brown, D. W. E. Allsopp, and W. B. Betts, IEEE Electron Device Lett. **34**, 66 (1998).
[9]J. Suehiro, R. Hamada, D. Noutomi, M. Shutou, and M. Hara, J. Electrost. **57**, 157 (2003).
[10]A. Sanchis, A. P. Brown, M. Sancho, G. Martinez, J. L. Sebastian, S. Munoz, and J. M. Miranda, Bioelectromagnetics **28**, 393 (2007).
[11]H. L. Dupont, C. L. Chappell, C. R. Sterling, P. C. Okhuysen, J. B. Rose, and W. Jakubowski, N. Engl. J. Med. **332**(13), 855 (1995).
[12]W. L. Current and L. S. Garcia, Clin. Microbiol. Rev. **4**(3), 325 (1991).
[13]S. Murugkar, C. L. Evans, X. S. Xie, and H. Anis, J. Microsc. **233**, 244 (2008).
[14]L. Wang, J. Lu, S. A. Marchenko, E. S. Monuki, L. A. Flanagan, and A. P. Lee, Electrophoresis **30**, 782 (2009).
[15]T. B. Jones, *Electromechanics of Particles* (Cambridge University Press, New York, 1995).
[16]C. Y. Yang and U. Lei, J. Appl. Phys **102**(094702), 1 (2007).
[17]J. Happel and B. Brenner, *Low Reynolds Number Hydrodynamics* (Dordrecht, Kluwer, 1983).
[18]A. Ramos, H. Morgan, N. G. Green, and A. Castellanos, J. Phys. D: Appl. Phys. **31**, 2338 (1998).
[19]A. D. Goater, J. P. H. Burt, and R. Pethig, J. Phys. D. Appl. Phys. **30**(18), L65 (1997).
[20]H. V. Smith, R. A. B. Nichols, and A. M. Grimason, Trends Parasitol. **21**(3), 133 (2005).
[21]A. L. Chatterjee, A. Carpentieri, D. M. Ratner, E. Bullitt, C. E. Costello, P. W. Robbins, and J. Samuelson, Giardia Cyst Wall Protein 1 Is a Lectin That Binds to Curled Fibrils of the GalNAc Homopolymer. **6**(8), 1 (2010).